IMPROVED ANALYSIS OF REMOTE SENSED DATA USING COMBINED PHYSICAL AND ENGINEERING APPROACHES

James J. Simpson
Digital Image Analysis Laboratory
Scripps Institution of Oceanography
University of California, San Diego

ABSTRACT

The accurate analysis of complex satellite scenes is a critical component of many environmental studies. Unfortunately, satellite data often contain noise of various kinds which can compromise scientific analysis. Moreover, a satellite scene generally contains information on many different space scales associated with a variety of geophysical and/or biogeochemical processes. Thus, an accurate segmentation of such scenes is an essential step prior to scientific analysis. Only after such steps (e.g., noise reduction, segmentation) have been done can meaningful geophysical analyses be performed. This paper shows the natural synogestic relationship between the engineering and scientific components of the aforementioned problems. The benefits obtained by such a combined approach are illustrated with specific examples (oceanic, atmospheric and terrestrial) using both polar orbiting and geostationary satellite data.

1. INTRODUCTION

Data collected by earth observing satellites (e.g., NOAA's Advanced Very High Resolution Radiometer (AVHRR); Geostationary Earth Observing Satellites (GOES)) are transmitted to earth in complex, band-interleaved data structures. Prior to use in quantitative scientific analyses, these data must be calibrated, geo-referenced, and segmented. Undetected clouds, for example, are the largest source of error (e.g., Robinson, 1985) in satellite derived estimates of sea surface temperature (SST) and thus proper segmentation of the data is an essential step prior to computing SST. Accurate calibration and segmentation, however, often are compromised by uncorrected sensor noise in the data.

Historically, many of these important steps either have not been done properly or in some cases, simply have not been done. This problem is exasperated by the fact that often scientists are unfamiliar with the relevant signal analysis and image segmentation techniques used in modern engineering disciplines. This paper documents through a few selected examples the benefits to be gained by the earth science community from incorporating more rigorous noise removal and segmentation procedures into the processing of remotely sensed satellite data prior to quantitative scientific analysis.

2. NOISE REMOVAL

2.1. GOES Visible Data

The periodic nature of the stripes in the GOES data (e.g., Weinreb *et al.*, 1989) suggests that finite impulse response (FIR) filters might prove successful in destriping the data. For each of the 81 GOES images analyzed, a mean one-dimensional power spectrum was computed by ensemble averaging 512 one-dimensional spectra taken down the columns of the image. As expected, the 81 ensemble averaged spectra show that noise in the GOES images associated with the stripes is narrow-band and isolated at frequencies of 1/8, 2/8, 3/8, and 4/8 cycles per pixel. The largest peak (at the highest frequency, 4/8 cycles per pixel) corresponds to the noise generated by the mismatch between every pair of adjacent lines. The smallest peak (at the lowest frequency, 1/8 cycles per pixel) corresponds to the slower, more regular eight line repeat cycle of the full sensor. This information provided the basis for the design of the target FIR filter used in this study. This filter can be implemented in three separate ways: 1) a one-dimensional Fourier FIR filtering of each of the N columns in the image; 2) equivalently as a single two-dimensional Fourier FIR filtering of the image; or 3) in the spatial domain by convolving segments of a given column with the spatial FIR filter kernel.

A one-dimensional target filter, consisting of narrow, frequency-targeted, one-dimensional wells placed at Fourier space coordinates 64, 128, 192 and a low pass filter starting at 240 (for the noise at 256 in the power spectrum) was constructed. These wells are constructed using one-dimensional Gaussian functions centered at the noise peaks in the power spectrum of the GOES data. For a N row by M column GOES scene, this one-dimensional Fourier implementation of the target filter must be applied N times. Moreover, some degree of signal mismatch can occur at column boundaries in the resultant filtered image because of the N independent Fourier calculations. For efficiency of the FFT calculations, this method imposes a power of two requirement on the vertical dimension of the image.

To circumvent some of these difficulties, a single two-dimensional Fourier implementation of the target filter can be applied to the GOES scene. This implementation of the target filter eliminates any potential mismatch at column boundaries between the N one-dimensional Fourier computations discussed above. The two-dimensional FFT requires a power of two in both dimensions of the image for efficiency.

Implementation of a one-dimensional spatial target FIR filter using the Parks-McClellan algorithm (McClellan *et al.*, 1973) simultaneously eliminates column boundary mismatch problems and removes power of 2 constraints on the dimensionality of the image. This latter feature makes it operationally more attractive than Fourier based implementations of the target filter. The Parks-McClellan algorithm uses a Chebyshev approximation to construct the desired filter impulse response. To remove stripes in the GOES imagery, the desired filter impulse response is specified in terms of a piecewise linear curve where the response is unity in the pass bands and zero in the stop bands. Stop bands are located at normalized

0-7803-2431-5/95 $4.00

frequencies of 0.25, 0.50, 0.75 and 1.0 (where the normalized Nyquist frequency is equal to 1). These frequencies correspond to periods of 2, 4, 8/3 and 8 pixels, respectively. With this specification as input to the Parks-McClellan algorithm, one can compute a set of coefficients that can be used to filter GOES data along columns in the spatial domain.

Once filter weights have been determined with the Parks-McClellan algorithm, only the length of the FIR filter kernel (i.e., the order of the filter) to be used in the convolution remains to be determined. This length was determined by comparing results obtained from a series of one-dimensional spatial FIR filters based on an inverse Fourier transform of the central column of the two-dimensional target transfer function. In taking a one-dimensional inverse FFT of the central column, we generate an "ideal" one-dimensional spatial filter of length 512. For computational efficiency, only a small number of these coefficients, selected symmetrically about the filter center, is needed. Analysis shows that a filter of length greater than 51 provides little signal to noise improvement but increases execution time.

Srinivasan *et al.* (1987) investigated a notch frequency domain filter for destriping Landsat data. A similar implementation using concentric rings constructed from two-dimensional Butterworth filters was evaluated for this study. It was rejected from further consideration because it tended to produce significant ringing in the filtered image. Moreover, the concentric notch design filtered along both spectral axes equally. The one-dimensional filtering effect of both target filter implementations is better suited to the one-dimensional nature of the stripes in GOES data.

2.2 AVHRR Mid-Infrared Data

The channel 3 data of the Advanced Very High Resolution Radiometer (AVHRR) on the NOAA series of weather satellites (NOAA 6-12) are contaminated by instrumentation noise. The signal to noise ratio (S/N) varies considerably from image to image and the between sensor variation in S/N can be large. Hence, the degree of filtering must be dependent upon the level of noise in the original data and the filter must be adaptive to variations in noise characteristics. For these reasons a Wiener filtering model was chosen for implementation.

A parametric Wiener filter model (1) is used to minimize the noise in AVHRR channel 3 data

$$S_o = H_w S_i \qquad (1)$$

where S_0 is the Fourier transform of the smoothed output signal and S_i is Fourier transform of the unfiltered input signal. The transfer function, H_w, is given by

$$H_w = \frac{1}{1 + \gamma \frac{P_n}{P_s}} \qquad (2)$$

where P_n is the estimated noise power spectrum, P_s is the estimated power spectrum of the uncorrupted signal, and γ controls the smoothing in the parametric Wiener filter (Castleman, 1979). For notational convenience, the frequency dependence of the Fourier transforms and power spectra (eqs. 1-3) is suppressed. As γ increases, more noise is removed but the amount of blurring in the image also is increased. Our tests indicate $\gamma = 1$ is a suitable choice. The primary difficulty in using the Wiener filtering model is making reasonable estimates of P_n and P_s.

Because the noise content of the channel 3 data varies from pass to pass, it is desirable that the noise power spectrum be independently estimated for the image. In estimating the noise spectrum, it is assumed that a significant amount of the noise energy is contained in the higher frequency components of the channel 3 image spectrum. This assumption is supported by the data (e.g., Simpson and Yhann, 1994). The Fourier transform of the noise, S_n, is estimated as the difference between the normalized Fourier transform of the unfiltered channel 3 data, $\bar{S}_i$, and the normalized Fourier transform of the low pass filtered channel 3 data, $\bar{S}_{ilp}$:

$$S_n = \bar{S}_i - \bar{S}_{ilp} \qquad (3)$$

The Fourier transforms are normalized because the estimated signal spectrum, as explained later, also is normalized. Because all spectra are normalized, the noise to signal ratio in (2) is maintained.

A circularly symmetric first order Butterworth low pass filter (Gonzalez and Wintz, 1977) is used to generate the Fourier transform of the low pass filtered channel 3 data, $\bar{S}_{ilp}$, from the Fourier transform of the unfiltered channel 3 data, S_i. The low pass filter bandwidth is in agreement with the dominant frequency components identified by Warren (1989) as being associated with the channel 3 noise[1]. A circularly symmetric low pass filter was chosen because the orientational preference of the noise is not necessarily well defined. The noise power spectrum is computed simply as: $P_n = S_n S_n^*$ where S_n^* is the complex conjugate of S_n. The noise power spectrum will contain some signal energy because of the circularly symmetric low pass filter used to generate $\bar{S}_{ilp}$. The effect of the signal energy in the noise power spectrum is partially mitigated by the presence of a good estimate for P_s (i.e., free of noise signal contamination).

The normalized channel 4 power spectrum is used as a noise free estimate of the normalized channel 3 power spectrum, which corresponds to the power spectrum of the uncorrupted signal, P_s. Use of the channel 4 spectrum is justified because both channels 3 and 4 have the same large-scale structure and they also show a high cross correlation over the ocean in the absence of channel 3 noise (Simpson and Yhann, 1994). Therefore, $P_s = \bar{S}_{ch4} \bar{S}_{ch4}^*$ where $\bar{S}_{ch4}$ is the normalized channel 4 Fourier transform and $\bar{S}_{ch4}^*$ is its complex conju-

1. Note, Warren uses wavelength instead of frequency to plot his Fourier transforms.

gate. Normalization of the energy spectra insures that the proper ratio is maintained between the noise spectrum computed from the channel 3 data and the signal spectrum estimated from the channel 4 data. This is necessary because channels 3 and 4 contain different amounts of total energy. Normalization therefore assigns equal amounts of energy to both the channel 3 and channel 4 signals. Note, it was necessary to introduce the channel 4 data as an estimate of the channel 3 data to make the filter defined by (2) signal dependent. Making use of the high correlation between the channel 3 and 4 data to estimate the signal power spectrum introduces the desired signal dependence into the Wiener filter design.

3. APPLICATIONS

3.1. Radiometric Calibration

The GOES-7 VISSR solar channels were radiometrically calibrated for the period from June 1987 through November 1988 (Frouin and Simpson, 1995). Space, White Sands, and the Sonora Desert are used as calibration targets. The calibration is performed in three different ways: 1) using the stretched data (i.e., retransmitted data operationally destriped using NOAA's normalization procedure) and considering individual VISSR detectors separately; 2) using the stretched data averaged over the 8 VISSR detectors; and 3) using the stretched data further destriped according to Simpson *et al.*, (1995) and then averaged over the 8 VISSR detectors (Figure 1). Because of uncertainties in the modeling of the VISSR radiance, using separate calibration coefficients for each detector (first approach) may not reduce the striping significantly. For best results, average calibration coefficients should be applied to data destriped according to Simpson *et al.* (1995).

3.2. Improved Cloud Detection

Examples of improved cloud discrimination which result from reduced noise in AVHRR channel 3 data, are shown in Figure 2. Simpson and Yhann (1994, Tables 3-5) also provide a quantitative comparison of the Wiener filter model with alternate noise reduction models (e.g. Minimum Mean Square Error with Conditional Markov model). The Wiener filtering model proved superior in all tests. The application of neural networks to cloud screening of AVHRR data over the ocean also was improved when the channel 3 noise was removed from the data prior to its use (Yhann and Simpson, 1995). Improved segmentation of sea ice from AVHRR scenes using fuzzy logic procedures also was significantly improved by filtering the channel 3 data prior to its use in the classifier (results not shown).

3.3. Robust Velocity Estimates

The maximum cross-correlation (MCC) method has been used to compute both oceanic and cloud velocity vectors from sequences of satellite data (e.g., Advanced Very High Resolution Radiometer (AVHRR), Coastal Zone Color Scanner (CZCS), Geostationary Observing Earth Satellite (GOES)). Unfortunately, the two dimensional cross-correlation functions used in the computation often contain saddle points which can give rise to large magnitude and direction uncertainties in the derived velocity estimates. A numerical iterative procedure was developed which combines image analysis methods (e.g., vector median filtering) and dynamical constraints to minimize these difficulties (Simpson and Gobat, 1994). The resultant velocities are both physically realistic and numerically stable. Thus, it also is possible to compute stream functions and simulated Lagrangian drifters. The validity of these results are confirmed with independent oceanic observations. Finally, the advective-diffusive equation is solved for a few oceanic applications (e.g., prediction of sea surface temperature, dispersal of anchovy eggs and larvae) using the derived velocities.

4. CONCLUSION

Analysis of satellite data for geophysical and biogeochemical applications can be improved by using engineering methods (e.g., noise reduction methods, image segmentation methods) prior to the specific scientific analysis.

REFERENCES

Castleman, D.R., 1979: Digital Image Processing, Englwood Cliffs, NJ: Prentice-Hall.

Frouin, R.J. and J.J. Simpson, 1995: Radiometric Calibration of VISSR Solar Channels during the GOES Pathfinder Benchmark Period, *Rem. Sens. Environ.*, in press.

Gallaudet, T.C. and J.J. Simpson, 1991: Automated Cloud Screening of AVHRR Imagery Using Split-and-Merge Clustering, *Rem. Sens. Environ.*, **38**, 77-121.

Gonzalez, R.C. and P. Wintz: 1977: Digital Image Processing. Reading, MA: Addison-Wesley.

McClellan, J.H., T.W. Parks and L.R. Rabiner, 1973: A computer program for designing optimal FIR linear phase digital filters. *IEEE Transactions on Audio and Electroacoustics*, AU-2, 506-526.

Robinson, I.S., 1985, Satellite Oceanography: an Introduction for Oceanographers and Remote-Sensing Scientists. Ellis Horwood Limited, New York, 455 pp.

Simpson, J.J. and S.R. Yhann, 1994: Reduction of Noise in AVHRR Channel 3 Data with Minimum Distortion, *IEEE Trans. Geo. Rem. Sens.*, **32**, 315-328.

Simpson, J.J. and J.I. Gobat, 1994: Robust Velocity Estimates, Stream Functions, and Simulated Lagrangian Drifters from Sequential Spacecraft Data, *IEEE Trans. Geo. Rem. Sens*, **32**, 479-493

Simpson, J.J., J.I. Gobat, R. Frouin, 1995: Improved Destriping of GOES Images using Finite Impulse Response Filters, *Rem. Sens. Environ.*, in press.

Srinivasan, R., M. Cannon, and J. White, 1987: Destriping of LandSat Data Using Power Spectral Filtering. Proceeding of SPIE Methods of Handling and Processing Imagery, 757, 34-39.

Warren, D. 1989: AVHRR Channel 3 Noise and Methods for its Removal, *Int. J. Remote Sensing*, **10**, 645-651.

Weinreb, M.P., R. Xie, J.H. Lienesch, and D.S. Crosby, 1989: Destriping GOES Images by Matching Empirical Distribution Functions. *Rem. Sens. Environ.*, **29**, 185-195.

Yhann, S.R. and J.J. Simpson, 1995: Application of Neural Networks to AVHRR Cloud Segmentation. *IEEE Trans. Geo. Rem. Sens.*, in press.

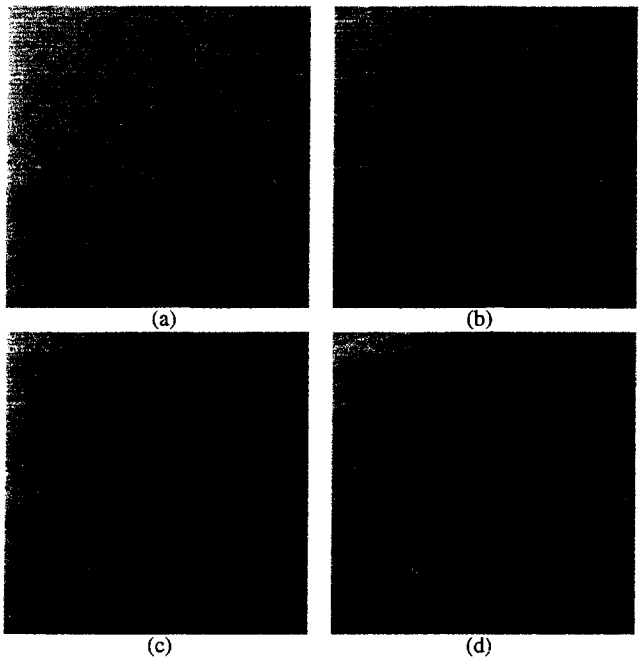

Figure 1: Raw and radiometrically calibrated VISSR image of White Sands. (a) raw image (count squared); (b) calibrated image using calibration coefficients of individual detectors; (c) calibrated average using calibration coefficients obtained by averaging count squared of striped data; and (d) calibrated image using calibration coefficients obtained by averaging count squared of destriped data. Gray scale is identical for all calibrated images. Data were destriped using the method of Simpson *et al.* (1995).

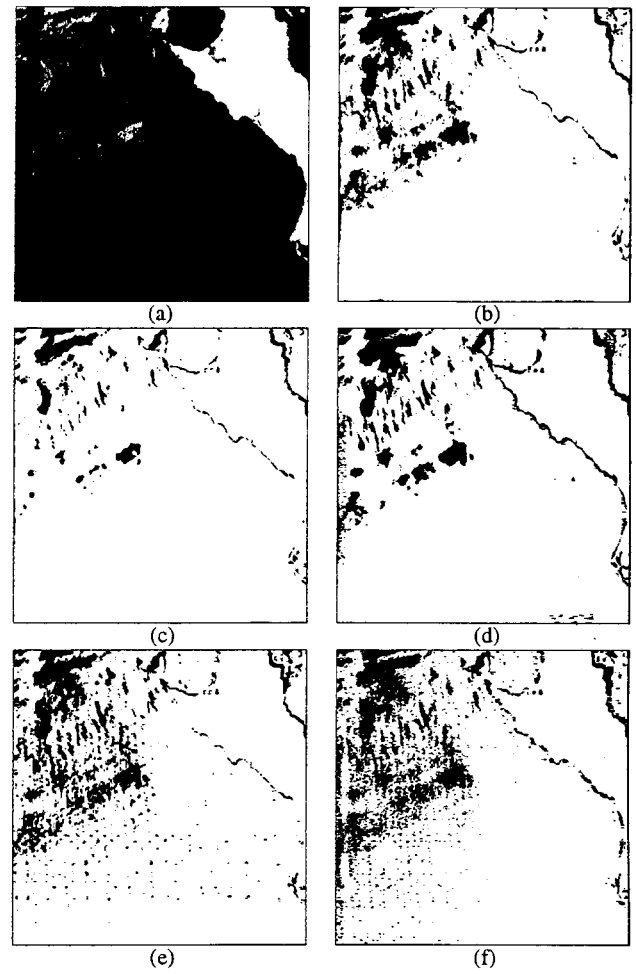

Figure 2: Result of applying PCTSMC cloud screen algorithm (Gallaudet and Simpson, 1991) to a typical AVHRR scene. a) Channel 2 data for the scene; cloud screen from b) Wiener filtered channel 3 (e.g., Simpson and Yhann, 1994); c) constrained least squares channel 3; d) interactive noise subtraction filtered channel 3; e) vertical 5×1 averaging filtered channel 3; and f) notch filtered channel 3. The cloud screened pixels in panels b-f also are shown in black.

ACKNOWLEDGEMENT

This work was supported by NASA. Special thanks to Program Managers J. Dodge and M. Maiden. Figure 1 is from Frouin and Simpson, (1995) with the destriping panel (d) done according to Simpson et al., 1995. Figure 2 is from Simpson and Yhann, 1994.